Iranian Journal of Medical Physics

ijmp.mums.ac.ir

A Method for Body Fat Composition Analysis in Abdominal Magnetic Resonance Images Via Self-Organizing Map Neural Network

Fatemeh Moghbeli[1], Mostafa Langarizadeh[1*], Ali Yoonesi[2], Amir Reza Radmard[3], Mohammad Sadegh Rahmanian[4], Azam Orooji[1]

1. Department of Health Information Management, School of Health Management and Information Sciences, Iran University of Medical Sciences, Tehran, Iran
2. Assistant Professor of Neuroscience, Faculty of Advanced Technologies in Medicine, Tehran University of Medical Sciences, Tehran, Iran
3. Department of Radiology, Shariati Hospital, Tehran University of Medical Sciences, Tehran, Iran
4. Department of Health Information Management, Faculty of Allied Medical Sciences, Tehran University of Medical Sciences, Faculty of Allied Medical Sciences Faculty of Allied Medical Sciences, Tehran, Iran

ARTICLE INFO

Article type:
Original Article

Article history:
Received: Sep 16, 2017
Accepted: Dec 15, 2017

Keywords:
Image Processing
Magnetic Resonance
Neural Network
Segmentation
Visceral Fat

ABSTRACT

Introduction: The present study aimed to suggest an unsupervised method for the segmentation of visceral adipose tissue (VAT) and subcutaneous adipose tissue (SAT) in axial magnetic resonance (MR) images of the abdomen.
Materials and Methods: A self-organizing map (SOM) neural network was designed to segment the adipose tissue from other tissues in the MR images. The segmentation of SAT and VAT was accomplished using a new level set method called distance regularized level set evolution (DRLSE). To evaluate the suggested method, the whole-body abdominal MRI was performed on 23 subjects, and three slices were selected for each case.
Results: The results of the automatic segmentation were compared with those of the manual segmentation and previous artificial intelligent methods. According to the results, there was a significant correlation between the automatic and manual segmentation results of VAT and SAT.
Conclusion: As the findings indicated, the suggested method improved detection of body fat. In this study, a fully automated abdominal adipose tissue segmentation algorithm was suggested, which used the SOM neural network and DRLSE level set algorithm. The proposed methodology was concluded to be accurate and robust with a significant advantage over the manual and previous segmentation methods in terms of speed and accuracy.

► *Please cite this article as:*
Moghbeli F, Langarizadeh M, Yoonesi A, Radmard AR, Rahmanian MS, Orooji A. A Method for Body Fat Composition Analysis in Abdominal Magnetic Resonance Images Via Self-Organizing Map Neural Network. Iran J Med Phys 2018; 15:108-116. 10.22038/ijmp.2017.26347.1265.

Introduction

The health practitioners universally acknowledge that excessive body fat is a serious health risk. Obesity is a risk factor for several chronic diseases, such as hypertension, hyperlipidemia, cardiovascular diseases, diabetes mellitus, gallbladder disease, respiratory failure, and a number of joint diseases [1, 2]. Moreover, according to the literature, the excessive accumulation of fat at particular parts of the body may be an important health risk factor [3]. Some other studies suggest that abdominal (body-center) fat pattern is more correlated with the metabolic risks associated with obesity than the gluteofemoral (peripheral) fat pattern.

These obesity problems have been attributed to an increase in visceral adipose tissue (VAT) and free fatty acid levels in the portal vein [4, 5]. According to several studies, VAT is responsible for the metabolic complications of obesity; furthermore, the subcutaneous adipose tissue (SAT) may contribute to the metabolic syndrome [6, 7]. Body composition can be evaluated through different methods ranging from field-based tests to advanced ones conducted in a clinical or laboratory setting by a professional technician.

The conventional methods of measuring the levels of adiposity include body mass index (BMI), waist circumference measurement, skinfold testing, bioelectrical impedance analysis, and BOD POD system (i.e., an Air Displacement Plethysmograph using whole body densitometry to characterize body composition [fat vs. lean]). The BOD POD is principally similar to underwater weighing and can measure body mass (weight) via a precise scale. The body

*Corresponding Author: Department of Health Information Management, School of Health Management and Information Sciences, Iran University of Medical Sciences, Tehran, Iran. No. 6, Rashid Yasami Ave., Vali-e-Asr St., Tehran, Iran. Tel: +989198616016, Email: langarizadeh.m@iums.ac.ir

volume is also estimated by sitting inside this device. The body density can be calculated through the following equation: [8, 9]

Density=Mass/Volume

It is difficult and imprecise to estimate the quantity and distribution of fat in human body, especially the volume and distribution of VAT around the internal organs. Currently, the most accurate and reliable methods for the qualitative and quantitative analysis of SAT and VAT are imaging techniques [10, 11]. Several imaging methods have been used for the calculation of abdominal fat distribution. One technique for the assessment of fat distribution, which represents a safer and more accurate noninvasive technique, compared to others, is magnetic resonance imaging (MRI).

In MRI, the area of a single abdominal slice is commonly analyzed; however, an accurate study of SAT and VAT requires multi-slice imaging [10]. The manual analysis of MRI slices is time-consuming and mostly depends on operators. Therefore, the development of computer-assisted methods can be a good idea to help analyze abdominal fat distribution. There are different studies targeting toward the segmentation of VAT and SAT from abdominal MRI data. The majority of the published studies are limited to techniques focusing on the abdomen using manual [12, 13], semiautomatic [13, 14], and fully automatic [13, 15, 16] approaches.

A number of these studies have used semiautomatic methods to measure adipose tissue in the whole-body MRI datasets [17-20]. However, the separation of the SAT from VAT is mainly performed by drawing borders around the VAT region manually. Nonetheless, the fully automatic approaches have been scarcely investigated for the segmentation and quantification of adipose tissue in whole-body MRI data [21, 22].

Kupusinac et al. used MATLAB, Version 7.11.0.584 (R2010b), to describe their methodology (i.e., the observed parameters and their measurements, the obtained dataset, and artificial neural network solution for predicting body fat), and reported the accuracy of 80.43%. In the mentioned study, body fat was predicted based on gender, age, and BMI by using artificial neural networks [23].

In the present study, we suggested an automatic approach for the segmentation of both SAT and VAT from abdominal T1-weighted MRI slices in a short time without any user interaction. This approach could facilitate an effective two-dimensional assessment of abdominal fat distribution. To this end, a self-organization map (SOM) neural network [24, 25] was designed to segment the total abdominal tissue (TAT) in the MRI slices. Subsequently, a new variation of level set formulation [26] was used to distinguish SAT and VAT from the total adipose tissue (TAT). Finally, the performance and accuracy of the suggested approach were compared with the manually-segmented MRI slices by a single expert radiologist at the baseline.

Materials and Methods

Subjects and Magnetic Resonance Imaging Protocol

A total of 23 unhealthy subjects, including 12 females and 11 males, with the age rage of 45-63 years voluntarily participated in this study. The subjects underwent a whole abdomen on a 1.5T unit (Symphony, Siemens, Erlangen, Germany) using an 8-channel phased array body coil with a T1-weighted spin echo pulse sequence (TR=100-120 msec/echo, TE=4.8 msec (IP) and 2.4 msec (OP), flip angle=70^{o}, slice thickness=8 mm). The field of view was 400 cm^2, the matrix was 256×160, and the imaging duration was 23 sec. Twenty axial slices were acquired from each subject covering the area from the lower lung to the level of L5/S1. The MR images were retrieved using the Digital Imaging and Communications in Medicine protocol.

Manual Image Segmentation

The manual segmentation of the MR images in all 23 subjects was performed by four experienced radiologists assessing the VAT and SAT compositions. Margins were drawn manually around SAT and VAT areas using a home-made software developed in MATLAB. The SAT and VAT areas were calculated through multiplying the pixel counts of segmented SAT and VAT by the MRI pixel area. The manual measurement of the fat deposits took approximately 10 min for each MRI slice in each subject. Because the process of manual segmentation was time-consuming, only slices in L4-L5, L3-L4, and L2-L3 levels were selected to be segmented manually. These segmented images were used as a gold standard for evaluating the automatic segmentation method.

Automated Image Segmentation

The standard sets of image processing tools, such as thresholding, morphological operations, intensity inhomogeneity correction, and level set algorithms, were used to perform the automated image analysis. The region growing algorithm was implemented in MATLAB via its image processing toolbox. The algorithm was designed with the aim of the robust segmentation of SAT and VAT without any user interaction during the execution of the algorithm. The segmented image data and area results were the output of the algorithm. The suggested automatic algorithm was based on the following six steps:

(1) Intensity inhomogeneity correction
(2) Body fat segmentation from background using SOM neural network

(3) Creation of the abdominal region of interest (ROI)
(4) Creation of SAT external wall mask using distance regularized level set evolution (DRLSE) algorithm
(5) Creation of SAT internal wall mask
(6) VAT and SAT identification

Each of these six steps is described in detail in the following subsections.

Intensity Inhomogeneity Correction

There are several sources of noise affecting MR images. Signal intensity inhomogeneity is one of these unavoidable artifacts also known as bias field. This artifact is mainly due to the inadequacies in the radiofrequency coils and object-dependent interactions [27-30]. Such intensity inhomogeneity is not a serious problem during clinical diagnosis and manual segmentation by radiologists. However, its associated impact can cause great difficulties for automatic intensity-based tissue classification methods.

Bias field artifact was observed in our acquired MR images. The technique chosen for removing the bias field effect was based on a solution proposed by Manjon et al. [31]. Figure 1 illustrates a slice in the presence of intensity inhomogeneity in the outer part of the SAT layer, along with its color map picture. Figure 2 depicts the same slice after performing the bias correction.

Body Fat Segmentation Using Self-Organizing Map Neural Network

Image segmentation can be performed through different techniques, which are mostly based on the discontinuity and similarity of the gray levels of an image. Artificial neural networks have been used in a variety of image processing applications. The SOM, usually known as Kohonen network, [32] is a computational technique that can visualize and analyze the high-dimensional data. The SOM can show a projection from a series of input data in a two-dimensional grid, and model m_i can be associated with each grid node (Figure 3).

These kinds of models are computed via SOM algorithm. A data item can be mapped onto the node having the most similar model to the data item, which has the shortest distance from the data item in some metrics. Although SOM is often used for reducing dimension, it has been also used for medical image segmentation [33]. The SOM neural network consists of two layers, the first and second layers of which include input neurons and output neurons (in form of two-dimensional grid view), respectively. Neurons in the input layer are connected to output layer neurons with an adjustable weight [34].

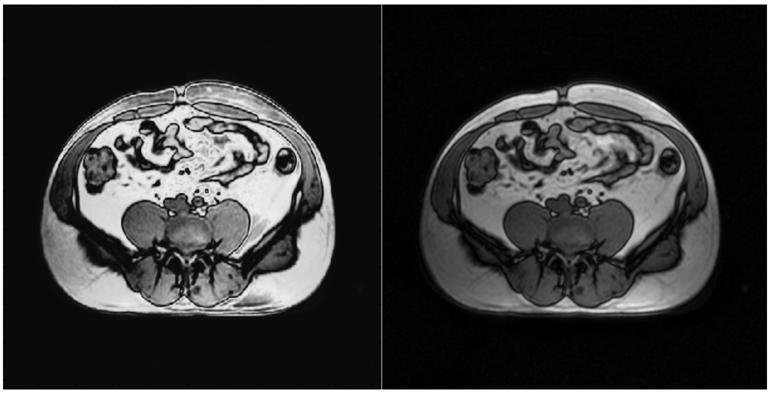

Figure 1. Magnetic resonance slice affected by bias field (left), gray scaled color map for the image (right)

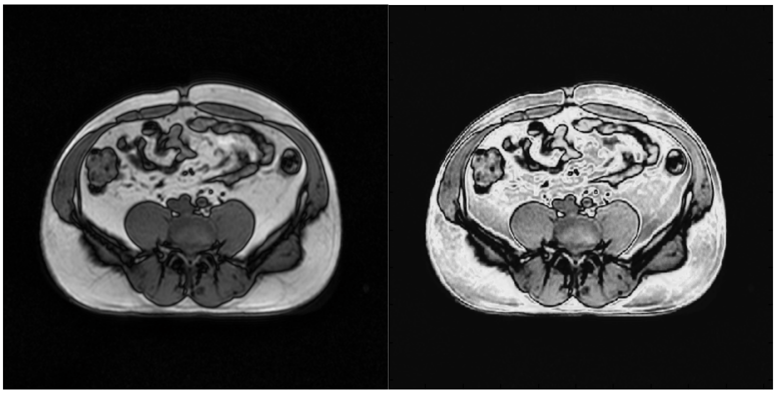

Figure 2. Bias field corrected slice (left), gray scaled color map for the image (right)

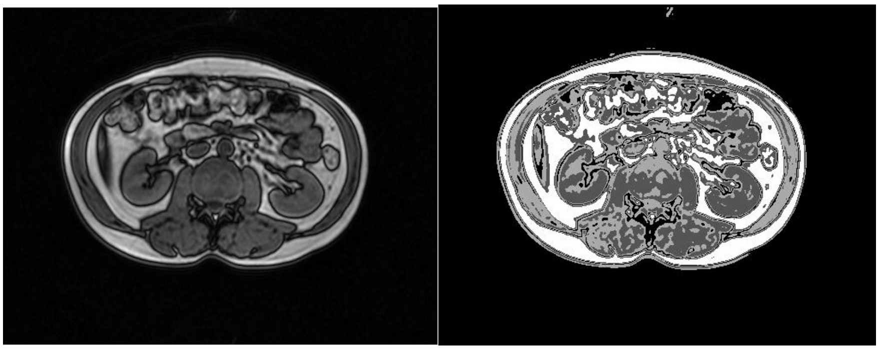

Figure 3. Input image to the self-organizing map network (left), segmented image (right)

In the SOM network, the most similar unit and winner neuron are determined by the minimum Euclidean distance to the input neurons. In this regard, x should be determined as the input vector and W_{ij} as the weight vector to the nodes. Input vector x is compared with all the weight vectors (W_{ij}). The best matching unit (BMU) or the winner node is determined by the smallest Euclidean distance (d_{ij}) as shown in Equation 1:

$$d_{ij} = \min \left\| x(t) - w_{ij}(t) \right\| \quad (1)$$

The modification of weight vector for the winner output neuron and its neighborhood neurons is calculated as:

$$w_{ij}(t+1) = w_{ij}(t) + \alpha(t)\left[x(t) - w_{ij}(t)\right] \ , \quad i \in N_c$$
$$w_{ij}(t+1) = w_{ij}(t) \ , \ i \notin N_c \quad (2)$$

where t stands for time, α is the gain sequence ($0<\alpha<1$), and N_c is the neighborhood of the neuron.

The training algorithm for the SOM network was as follows:

1. Initialization of each node weights
2. Choosing a vector randomly from the input training data
3. Examining every node to determine the node weights with the most similarity to the input vector; the node whose weights have the smallest distance from the input vector is determined as the wining node or BMU
4. Calculating BMU neighborhood; the amount of neighborhood is decreasing over the time.
5. Updating the BMU and its neighborhood weight according to Equation 2.
6. If $N_c \neq 0$, then go to step 2.

Our SOM network for the MRI tissue segmentation had one neuron in the input layer and four neurons in the output layer in form of a 2×2 grid. The reason for selecting four neurons in the output layer was due to having four tissues in the T1-wieghted input MRI, including air and water, bone marrow, fat, and muscles. We reshaped n×m MRI image to 1×(m×n) matrix in order to send the image as the input signal to the network. Random pixels were selected from the image to be used in the network training process.

It has been observed that the use of only a small fraction of image pixels provides sufficient segmentation results. Therefore, in the training stage, a few image pixels were taken into account rather than taking all image pixels. When the training stage was over, we could use the network to segment the other remaining MR images. Figure 4 illustrates the input image (TAT mask [all voxels of the noise-masked fat-fraction map]) [35]) to the network and its segmentation result.

After the segmentation of the input image into its four areas, we needed to segment the TAT from the segmented image. The segmentation result indicated that TAT (white area) had the maximum number of pixels standing next to the air and water area (black). Therefore, the TAT could be segmented by the selection of the pixels having the second maximum value as their label. Figure 4 displays the segmented TAT.

Creation of the Abdominal Region of Interest

After the creation of the total abdominal tissue mask, we needed to identify the rectangular region of interest (ROI) only in the abdomen. This facilitated the reduction of the calculation time in the next steps by decreasing the number of pixels to be processed. The vertical and horizontal boundary detection is depicted in Figure 5. In order to obtain the ROI mask coordination, we could easily find the starting and ending points of each calculated sum plot. The obtained mask is displayed in Figure 6.

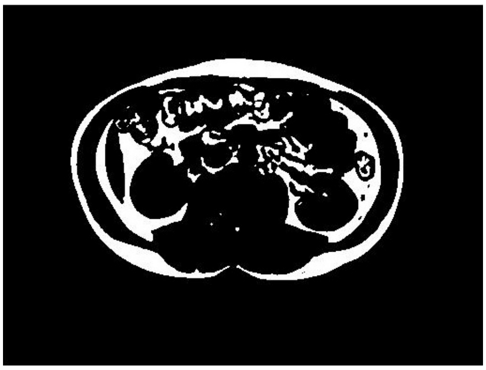

Figure 4. Total adipose tissue mask

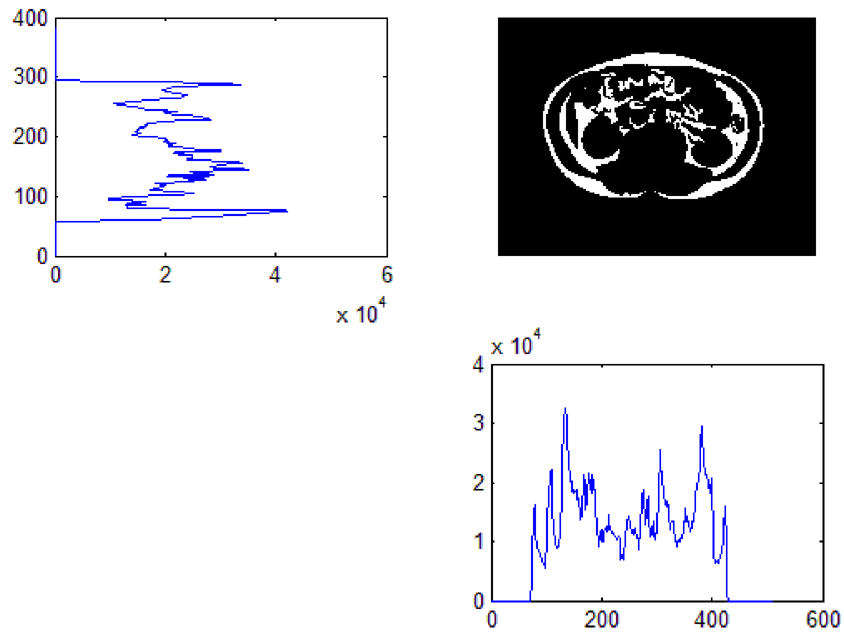

Figure 5. Row and column sums

Figure 6. Abdominal region of interest mask

Creation of Subcutaneous Adipose Tissue External Wall Mask Using the Distance Regularized Level Set Evolution Algorithm

Level set methods have been widely used in capturing dynamic interfaces and shapes in images. Level set algorithm is based on representing a contour as the zero level set of a higher dimensional function called 'level set function', followed by formulating the motion of the contour as the evolution of the level set function [36, 37]. The main advantage of active contour models is their ability to represent complex topologies and handle topological changes. Active contour model was formulated in terms of a dynamic parametric contour as expressed in Equation 3:

$$C(s,t):[0,1]\times[0,\infty)\rightarrow\Re^2 \qquad (3)$$

where the spatial parameter s ($s\epsilon[0, 1]$) parameterizes the points in the contour, and t is the temporal variable in $[0, \infty)$. The evolution of the curve was expressed in Equation 4.

$$\partial C(s,t)/\partial t = F\mathcal{N} \qquad (4)$$

where F is the speed function, and $\mathcal{N}$ is the internal normal vector to the curve C.

The curve evolution in Equation 4 can be converted to a zero level set of time-dependent level set function as $\varphi(x, y, t)$. The level set function of φ is assumed to get negative values inside the zero level set contour and positive values outside the contour. The internal normal vector of $\mathcal{N}$ was expressed in Equation 5.

$$\mathcal{N} = -\nabla\phi/|\nabla\phi| \qquad (5)$$

Finally, the curve equation in Equation 4 was converted to the following partial differential equation, called 'level set evolution' equation.

$$\partial\phi/\partial t = F|\nabla\phi| \qquad (6)$$

In the conventional level set formulation described earlier, irregularities can rise in the level set function during its evolution causing numerical errors. This may finally destroy the stability of the evolution. Some numerical remedies to this problem have been proposed [38, 39]; nonetheless, they have their own problems, such as affecting numerical accuracy in an undesirable way.

Chunming et al. [26] proposed a new variation of level set formulation in which the level set function regularity was essentially maintained during the level set evolution known as DRLSE. This suggested method does not have the previously mentioned numerical errors. We utilized DRLSE method to get the contour of the SAT outer wall (for more information about DRLSE method, refer to [26]). We also implemented the DRLSE algorithm on the TAT mask with the required initial mask of rectangular

ROI created from the previous step. Some of the DRLSE steps and the final contour of SAT outer wall mask are presented in Figure 7.

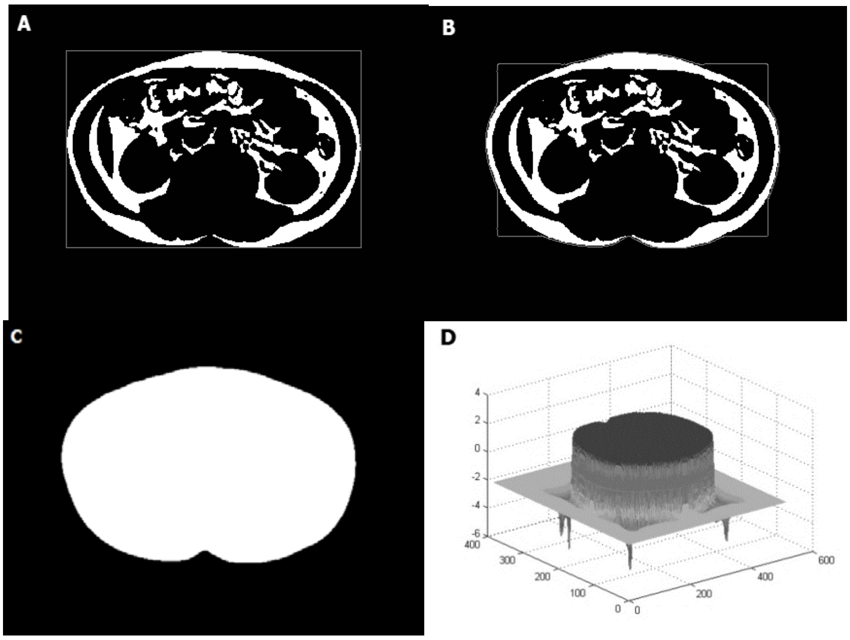

Figure 7. (A) Initial level set contour, (B) level set contour after 100 iterations, (C) final subcutaneous adipose tissue outer wall mask, (D) final level set function

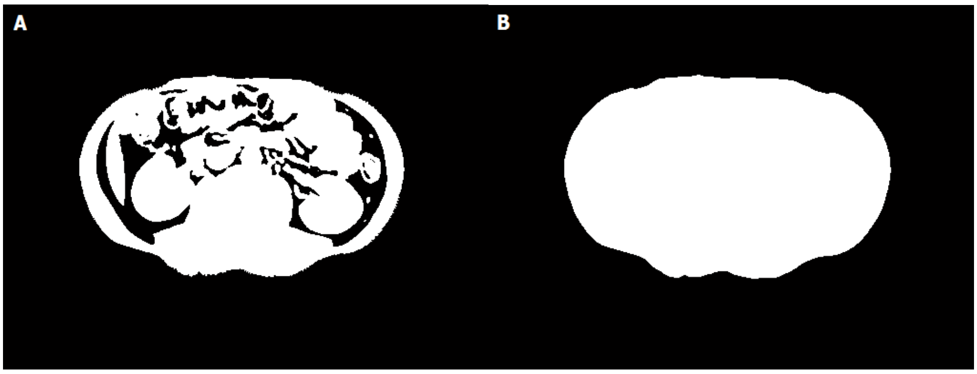

Figure 8. A) Obtained non-fat mask, B) subcutaneous adipose tissue internal wall mask

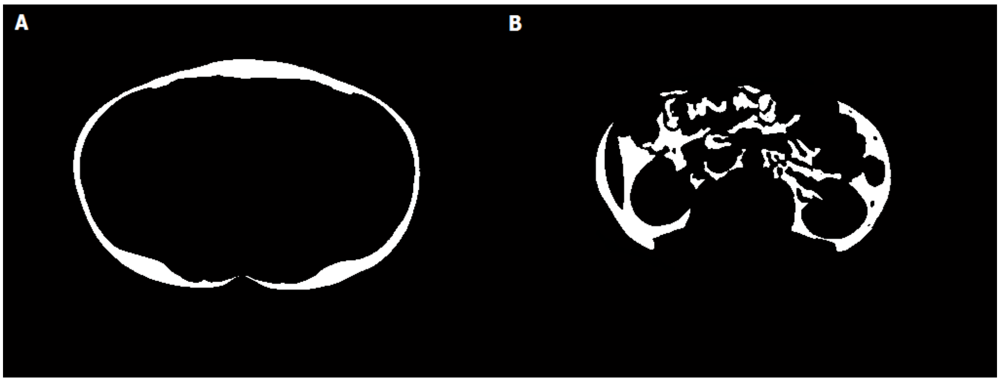

Figure 9. A) Obtained subcutaneous adipose tissue mask, B) obtained visceral adipose tissue mask

Creation of Subcutaneous Adipose Tissue Internal Wall Mask

After the creation of the SAT outer wall mask, the SAT internal wall mask was created in order to identify SAT and VAT from the TAT. To this end, the non-fat tissue obtained from the TAT mask was created. Subsequently, the DRLSE algorithm was run on the obtained mask to get the SAT internal wall. To create the non-fat tissue mask, we simply multiplied the mask of the SAT outer wall obtained from the previous step by the inverted TAT mask. The non-fat tissue mask and the SAT internal wall mask obtained from the DRLSE algorithm are demonstrated in Figure 8.

Identification of Visceral and Subcutaneous Adipose Tissues

To identify the SAT from the TAT mask, the obtained SAT internal wall mask was subtracted from the SAT outer wall mask created in step 4. The VAT mask could be obtained by subtracting the estmated SAT mask from the TAT mask. The equations used for the identification of SAT and VAT were as follows.

$$SAT = SAT_{outer\ wall\ mask} - SAT_{internal\ wall\ mask} \quad (7)$$

$$VAT = TAT - SAT \quad (8)$$

The obtained results are shown in Figure 9.

Results

In order to measure the effectiveness of the suggested method, the data acquired from the automatic segmentation were compared to the manual segmentation results performed by four experienced radiologists and other methods (Table 1). A total of 69 images, obtained from 23 subjects (each having three images), were segmented with both manual and automatic methods. The sum of VAT and SAT in three slices were calculated in both methods.

The correlation between the results of the automatic and manual segmentation for SAT and VAT was calculated. Regarding the SAT results, the two approaches showed a high correlation (r=0.9082, P<0.001). There was also a high correlation between the two approaches in terms of the VAT results (r=0.8988, P<0.001). The Bland-Altman plots for both VAT and SAT assessments are illustrated in Figure 10.

The SAT and VAT areas calculated using automatic method were slightly higher than those estimated manually. This was due to the fact that the operator usually dismisses very thin areas, especially in VAT, while the automatic method considers every pixel in an image for both tissues.

Discussion

This study revealed the possibility of performing fully automated segmentation of SAT and VAT from abdominal MR images. Unlike SAT, the segmentation of VAT is a difficult and less accurate task due to its complex structure. The segmentation process is usually performed in several steps each of which is related to the results of the previous steps. The bias correction step in our study is a critical stage that can affect the whole segmentation process. Therefore, we utilized a robust and accurate method proposed by Manjon et al. [31] to overcome this problem. This method fully corrected the bias field effect as presented in our data.

In the majority of the investigations, segmenting fat from T1-weighted MR images has been accomplished by thresholding or using fuzzy clustering method [10, 15, 17, 21, 43]. The main drawback of the thresholding method is its requirement for different thresholds and needing additional time to calculate the threshold for each slice. Fuzzy clustering method is also a robust technique in image segmentation, which is based on the similarities in pixel intensity. The main disadvantage of this method is that it needs to calculate the membership functions in every slice, which takes time similar to the thresholding method.

In our suggested method, we trained a SOM neural network for the first time, and then used the trained network to segment all the remaining slices. In this regard, we reduced the time needed to segment fat from other tissues. After distinguishing adipose tissue types by means of the suggested method via DRLSE level algorithm, a comparison was made between the manually segmented images and the automatically segmented ones. The areas calculated for VAT were significantly different from the manual SAT results due to the high precision of algorithm in counting every pixel of the VAT ignored in the manual segmentation.

Table 1. Comparison of automatic and manual segmentation results

Row	Method	Result	Reference
1	Artificial Neural Network (ANN)	ANN solution for predicting Body Fat with accuracy 80.43%	[23]
2	Photoshop software and ANOVA correlation by SPSS	Correlation VAT: r^2=0.753; required time: 6 min	[40]
3	Manual method	Correlation VAT: r^2=0.784; required time: 2 h	[40]
4	Fuzzy clustering algorithm	Correlation VAT: r^2=0.9601; required time: 6 min	[41]
5	Non-rigid registration	Correlation VAT: r^2=0.7781; required time: 1 h	[42]

Conclusion

It can be concluded that the suggested method enhanced detection of body fat. In this study, a fully automated abdominal adipose tissue segmentation algorithm was suggested, which entailed the use of the SOM neural network and DRLSE level set algorithm. The proposed methodology was found to be precise and robust with a significant advantage over the manual segmentation and other methods in terms of speed and accuracy. This method allows for the segmentation of the whole abdominal fat in the MR images without any user interaction. It also provides useful clinical means for characterizing abdominal fat compositions.

References

1. Kravitz L, Heyward VH. Getting a grip on body composition. IDEA today. 1992;10:34-41.
2. Safdari R, Kadivar M, Langarizadeh M, Nejad A, Kermani F. Developing a fuzzy expert system to predict the risk of neonatal death. Acta Informatica Medica. 2016;24(1):34-7.
3. WILIMORE J, Buskirk E, DiGirolamo M, Lohman T. BODY-COMPOSITION-A ROUND-TABLE. PHYSICIAN AND SPORTSMEDICINE. 1986;14(3):144-&.
4. Smith SR, Lovejoy JC, Greenway F, Ryan D, deJonge L, de la Bretonne J, et al. Contributions of total body fat, abdominal subcutaneous adipose tissue compartments, and visceral adipose tissue to the metabolic complications of obesity. Metabolism. 2001;50(4):425-35.
5. Björntorp P. " Portal" adipose tissue as a generator of risk factors for cardiovascular disease and diabetes. Arteriosclerosis, Thrombosis, and Vascular Biology. 1990;10(4):493-6.
6. Seidell J, Bouchard C. Visceral fat in relation to health: is it a major culprit or simply an innocent bystander? International journal of obesity and related metabolic disorders: journal of the International Association for the Study of Obesity. 1997;21(8):626-31.
7. Abate N, Garg A, Peshock RM, Stray-Gundersen J, Adams-Huet B, Grundy SM. Relationship of generalized and regional adiposity to insulin sensitivity in men with NIDDM. Diabetes. 1996;45(12):1684-93.
8. Heyward VH, Wagner DR. Applied body composition assessment. 2004.
9. Otterstetter R, Johnson K, Kiger D, Agnor S, Edwards J, Naylor J, et al. The effect of acute moderate-intensity exercise on the accuracy of air-displacement plethysmography in young adults. European journal of clinical nutrition. 2013;67(10):1092-4.
10. Abate N, Burns D, Peshock R, Garg A, Grundy SM. Estimation of adipose tissue mass by magnetic resonance imaging: validation against dissection in human cadavers. Journal of lipid research. 1994;35(8):1490-6.
11. Iacobellis G. Imaging of visceral adipose tissue: an emerging diagnostic tool and therapeutic target. Current Drug Targets-Cardiovascular & Hematological Disorders. 2005;5(4):345-53.
12. Shen W, Punyanitya M, Wang Z, Gallagher D, St-Onge M-P, Albu J, et al. Visceral adipose tissue: relations between single-slice areas and total volume. The American journal of clinical nutrition. 2004;80(2):271-8.
13. Bonekamp S, Ghosh P, Crawford S, Solga S, Horska A, Brancati F, et al. Quantitative comparison and evaluation of software packages for assessment of abdominal adipose tissue distribution by magnetic resonance imaging. International Journal of Obesity. 2008;32(1):100-11.
14. Armao D, Guyon JP, Firat Z, Brown MA, Semelka RC. Accurate quantification of visceral adipose tissue (VAT) using water-saturation MRI and computer segmentation: Preliminary results. Journal of Magnetic Resonance Imaging. 2006;23(5):736-41.
15. Kullberg J, Ahlström H, Johansson L, Frimmel H. Automated and reproducible segmentation of visceral and subcutaneous adipose tissue from abdominal MRI. International Journal of Obesity. 2007;31(12):1806-17.
16. Kullberg J, Karlsson AK, Stokland E, Svensson PA, Dahlgren J. Adipose tissue distribution in children: automated quantification using water and fat MRI. Journal of Magnetic Resonance Imaging. 2010;32(1):204-10.
17. Brennan DD, Whelan PF, Robinson K, Ghita O, O'Brien JM, Sadleir R, et al. Rapid automated measurement of body fat distribution from whole-body MRI. American Journal of Roentgenology. 2005;185(2):418-23.
18. Machann J, Thamer C, Schnoedt B, Haap M, Haring HU, Claussen CD, et al. Standardized assessment of whole body adipose tissue topography by MRI. Journal of Magnetic Resonance Imaging. 2005;21(4):455-62.
19. Machann J, Thamer C, Stefan N, Schwenzer NF, Kantartzis K, Häring H-U, et al. Follow-up Whole-Body Assessment of Adipose Tissue Compartments during a Lifestyle Intervention in a Large Cohort at Increased Risk for Type 2 Diabetes 1. Radiology. 2010;257(2):353-63.
20. Moghbeli F, Langarizadeh M, Aliabadi A. Application of Ethics for Providing Telemedicine Services and Information Technology. Medical Archives. 2017;71(5):351-5.
21. Kullberg J, Johansson L, Ahlström H, Courivaud F, Koken P, Eggers H, et al. Automated Assessment of whole-body adipose tissue depots from continuously moving bed MRI: A feasibility study. Journal of Magnetic Resonance Imaging. 2009;30(1):185-93.
22. Würslin C, Machann J, Rempp H, Claussen C, Yang B, Schick F. Topography mapping of whole body adipose tissue using a fully automated and standardized procedure. Journal of Magnetic Resonance Imaging. 2010;31(2):430-9.

23. Kupusinac A, Stokić E, Doroslovački R. Predicting body fat percentage based on gender, age and BMI by using artificial neural networks. Computer methods and programs in biomedicine. 2014;113(2):610-9.
24. Chang P-L, Teng W-G, editors. Exploiting the self-organizing map for medical image segmentation. Computer-Based Medical Systems, 2007 CBMS'07 Twentieth IEEE International Symposium on; 2007: IEEE.
25. Langarizadeh M, Moghbeli F. Applying naive bayesian networks to disease prediction: a systematic review. Acta Informatica Medica. 2016;24(5):364.
26. Li C, Xu C, Gui C, Fox MD. Distance regularized level set evolution and its application to image segmentation. Image Processing, IEEE Transactions on. 2010;19(12):3243-54.
27. Sled JG, Zijdenbos AP, Evans AC. A nonparametric method for automatic correction of intensity nonuniformity in MRI data. Medical Imaging, IEEE Transactions on. 1998;17(1):87-97.
28. Langarizadeh M, Mahmud R, Ramli A, Napis S, Beikzadeh M, Rahman WWA. Effects of enhancement methods on diagnostic quality of digital mammogram images. Iranian Journal of Cancer Prevention. 2012;3(1):36-41.
29. Jangi M, Fernández-de-las-Peñas C, Tara M, Moghbeli F, Ghaderi F, Javanshir K. A systematic review on reminder systems in Physical therapy. Caspian Journal of Internal Medicine. 2018;9(1):2-0.
30. Langarizadeh M, Maghsoudi B, Nilforushan N. Decision support system for age-related macular degeneration using convolutional neural networks. Iranian Journal of Medical Physics. 2017;14(3):141-8.
31. Manjón JV, Lull JJ, Carbonell-Caballero J, García-Martí G, Martí-Bonmatí L, Robles M. A nonparametric MRI inhomogeneity correction method. Medical Image Analysis. 2007;11(4):336-45.
32. Kohonen T. Self-organized formation of topologically correct feature maps. Biological cybernetics. 1982;43(1):59-69.
33. Rickard HE, Tourassi GD, Eltonsy N, Elmaghraby AS, editors. Breast segmentation in screening mammograms using multiscale analysis and self-organizing maps. Engineering in Medicine and Biology Society, 2004 IEMBS'04 26th Annual International Conference of the IEEE; 2004: IEEE.
34. Demirhan A, Güler İ. Combining stationary wavelet transform and self-organizing maps for brain MR image segmentation. Engineering Applications of Artificial Intelligence. 2011;24(2):358-67.
35. Poonawalla AH, Sjoberg BP, Rehm JL, Hernando D, Hines CD, Irarrazaval P, et al. Adipose tissue MRI for quantitative measurement of central obesity. Journal of Magnetic Resonance Imaging. 2013;37(3):707-16.
36. Caselles V, Catté F, Coll T, Dibos F. A geometric model for active contours in image processing. Numerische mathematik. 1993;66(1):1-31.
37. Malladi R, Sethian JA, Vemuri BC. Shape modeling with front propagation: A level set approach. Pattern Analysis and Machine Intelligence, IEEE Transactions on. 1995;17(2):158-75.
38. ng methods. Journal of Computing and Information Technology. 2003;11(1):1-2.
39. Fedkiw SOR. Level set methods and dynamic implicit surfaces. 2003.
40. Gronemeyer SA, Steen RG, Kauffman WM, Reddick WE, Glass JO. Fast adipose tissue (FAT) assessment by MRI. Magnetic resonance imaging. 2000;18(7):815-8.
41. Positano V, Gastaldelli A, Santarelli MF, Lombardi M, Landini L. An accurate and robust method for unsupervised assessment of abdominal fat by MRI. Journal of Magnetic Resonance Imaging. 2004;20(4):684-9.
42. Joshi AA, Hu HH, Leahy RM, Goran MI, Nayak KS. Automatic intra-subject registration-based segmentation of abdominal fat from water–fat MRI. Journal of Magnetic Resonance Imaging. 2013;37(2):423-30.
43. Nilashi M, Ibrahim O, Ahmadi H, Shahmoradi L. A knowledge-based system for breast cancer classification using fuzzy logic method. Telematics and Informatics. 2017;34(4):133-44.